

Random noise attenuation by f - x empirical mode decomposition predictive filtering ^a

^aPublished in Geophysics, 79, no. 3, V81-V91, (2014)

Yangkang Chen and Jitao Ma†*

ABSTRACT

Random noise attenuation always plays an important role in seismic data processing. One of the most widely used methods for suppressing random noise is $f - x$ predictive filtering. When the subsurface structure becomes complex, this method suffers from higher prediction errors owing to the large number of different dip components that need to be predicted. In this paper, we propose a novel denoising method termed $f - x$ empirical mode decomposition predictive filtering (EMDPF). This new scheme solves the problem that makes $f - x$ empirical mode decomposition (EMD) ineffective with complex seismic data. Also, by making the prediction more precise, the new scheme removes the limitation of conventional $f - x$ predictive filtering when dealing with multi-dip seismic profiles. In this new method, we first apply EMD to each frequency slice in the $f - x$ domain and obtain several intrinsic mode functions (IMF). Then an autoregressive (AR) model is applied to the sum of the first few IMFs, which contain the high-dip-angle components, in order to predict the useful steeper events. Finally, the predicted events are added to the sum of the remaining IMFs. This process improves the prediction precision by utilizing an EMD based dip filter to reduce the dip components before $f - x$ predictive filtering. Both synthetic and real data sets demonstrate the performance of our proposed method in preserving more useful energy.

INTRODUCTION

Further development of exploration and production of reservoirs increases the demand for random noise suppression. Current random noise attenuation methods are realized in either the $t - x$ or a transformed domain (Liu et al., 2009c). In the $t - x$ domain, denoising methods include stacking (Mayne, 1962; Yilmaz, 2001; Liu et al., 2009a), polynomial fitting (Zhong et al., 2006; Liu et al., 2011), and median filtering (Liu et al., 2007). All these methods fully utilize the differences of both travel time and apparent velocity between signal and noise in the $t - x$ domain. In transformed domains, denoising methods include $f - x$ predictive filtering (Canales, 1984), the wavelet transform (Zhang and Ulrych, 2003; Gao et al., 2006), the curvelet transform (Neelamani et al., 2008), and the seislet transform (Liu et al., 2009b; Fomel and Liu,

2010). These methods transform the seismic data from the $t - x$ domain to some other domain, where the signal and random noise can be separated. The noise is removed in the transformed domain prior to transformation back to the $t - x$ domain.

Canales (1984) first used $f - x$ predictive filtering to attenuate random noise. Since then, continuous efforts have been made to improve the predictive precision or to modify the conventional version to meet better the requirements set by various applications. Guo et al. (1995) proposed $f - xy$ predictive filtering in order to improve the adaptation to both 2D and 3D post-stack seismic data processing. Su et al. (1998) suggested $f - xyz$ predictive filtering, which is mainly used for random noise attenuation in a pre-stack data set. Kang et al. (2003) proposed a $f - x$ quasi-linear transform method adapted to the non-linear events of seismic data in complex regions. Unfortunately, when the subsurface is extremely complex, $f - x$ predictive filtering does not yield good results because of the large number of dip components that need to be predicted.

Huang et al. (1998) proposed a new signal processing method, which uses empirical mode decomposition (EMD) to prepare stable input for the Hilbert Transform. The essence of EMD is to stabilize a non-stationary signal. That is, to decompose a signal into a series of intrinsic mode functions (IMF). Each IMF has a relatively local-constant frequency. The frequency of each IMF decreases according to the separation sequence of each IMF. EMD is a breakthrough in the analysis of linear and stable spectra. It adaptively separates non-linear and non-stationary signals, which are features of seismic data, into different frequency ranges. Bekara and van der Baan (2009) applied $f - x$ EMD to attenuation of random and coherent noise, with good results. Cai et al. (2011) suggested using $t - f - x$ EMD to denoise seismic data on the basis of a mixed time-frequency analysis. Nevertheless, for the purpose of random noise attenuation, the $f - x$ and $t - f - x$ domain EMD methods can only be applied on NMO corrected or post-stack seismic data. With profiles containing dipping events, these methods will suppress some of the useful energy.

In this paper, we propose a new approach, termed $f - x$ empirical mode decomposition predictive filtering (EMDPF), which combines both $f - x$ EMD and $f - x$ predictive filtering. This new noise attenuation methodology can adapt to more complex seismic profiles than $f - x$ EMD and preserve more useful energy than $f - x$ predictive filtering. $f - x$ EMDPF uses an EMD based dip filter to reduce the dip components for the subsequent predictive filtering in order to improve the predictive precision.

We start this paper by reviewing the conventional $f - x$ predictive filtering theory and point out its high-prediction-error problem when the number of dip components becomes large. Then we review basic EMD theory and its application, both in data processing and the exploration geophysical fields. Finally, we suggest a way to combine the properties of both $f - x$ predictive filtering and $f - x$ EMD in order to form the new denoising algorithm, $f - x$ EMDPF. Three synthetic data sets and one real data set demonstrate that $f - x$ EMDPF can preserve much more useful energy while removing slightly less random noise than $f - x$ EMD and $f - x$ predictive filtering.

***F-X* PREDICTIVE FILTERING**

Let $s(t, h)$ ($h = 1, 2, \dots, H$) be the signal of trace h and H be the number of traces. If the slope of a linear event with constant amplitude in a seismic section is ψ , then:

$$s(t, h + 1) = s(t - h\psi\Delta x, 1), \quad (1)$$

where Δx denotes the trace interval. Equation 1 can be transformed into the frequency domain in order to give:

$$S(f, h + 1) = S(f, 1)e^{-i2\pi fh\psi\Delta x}. \quad (2)$$

For a specific frequency f_0 , from equation 2 we can obtain a linear recursion, which is given by:

$$S(f_0, h + 1) = a(f_0, 1)S(f_0, h), \quad (3)$$

where $a(f_0, 1) = e^{-i2\pi f_0\psi\Delta x}$. This recursion is a first-order difference equation, also known as an auto-regressive (AR) model of order 1. Similarly, superposition of p linear events in the $t - x$ domain can be represented by an AR model of order p (Tufts and Kumaresan, 1980; Harris and White, 1997) as the following equation:

$$S(f_0, h + 1) = a(f_0, 1)S(f_0, h) + a(f_0, 2)S(f_0, h - 1) + \dots + a(f_0, p)S(f_0, h + 1 - p), \quad (4)$$

where $a(f_0, h)$ ($h = 1, 2, \dots, p$) denotes the predictive error filter, with a length of p . The prediction error energy $E(f_0)$ is given by the following equation:

$$E(f_0) = \|a(f_0, h) * S(f_0, h) - S(f_0, h + 1)\|_2^2, \quad (5)$$

where symbol $*$ denotes convolution, and $\|\cdot\|_2^2$ denotes the least-squares energy. By minimizing the prediction error energy $E(f_0)$, we can get the filtering operator $a(f_0, m)$. Applying this operator to the spatial trace yields the denoised results for the frequency slice f_0 .

$f - x$ predictive filtering works perfectly on a single event. Figures 1a-1c show and compare the denoised results for a single flat synthetic event. The denoised result (Figure 1b) is quite good, with the random noise in Figure 1a largely removed and only a small amount of the useful component in the noise section, Figure 1c. For a single dipping event, Figures 1d-1f, the results are similar. However, when the number of different dips is increased, the seismic section becomes more complex and predictive filtering is not as effective. Figure 1j shows a synthetic section containing four events with differing dips. In the removed noise section, Figure 1i, there remains a significant amount of residual useful energy.

The synthetic data shown in Figures 1a, 1d, and 1j were all generated by SeismicLab (Sacchi, 2008), with a signal-to-noise ratio (SNR) of 2.0 for all of them. Here we define the SNR as the ratio of maximum amplitude of useful energy and the maximum amplitude of Gaussian white noise. Note that the same parameters were used for the predictive filters in each case shown in Figure 1.

We now conclude that the effectiveness of $f - x$ predictive filtering deteriorates as the number of different dips increases, mainly because the total of leaked useful energy increases at the same time. In particular, when the number of dips is extremely large, as occurs with hyperbolic events, $f - x$ predictive filtering fails to achieve acceptable results. It is natural to infer that if we can first reduce the number of dips, or in other words pick the very steep events and total random noise out, then by applying the same $f - x$ predictive filtering, the predictive precision will improve. That is the subject of the section on $f - x$ empirical mode decomposition predictive filtering.

EMPIRICAL MODE DECOMPOSITION

1D EMD

The aim of empirical mode decomposition (EMD) is to empirically decompose a non-stationary signal into a finite set of subsignals, which are termed intrinsic mode functions (IMF) and are considered to be stable. The IMFs satisfy two conditions: (1) in the whole data set, the number of extrema and the number of zero crossings must either equal or differ at most by one; and (2) at any point, the mean value of the envelope defined by the local maxima and the envelope defined by the local minima is zero (Huang et al., 1998).

Provided that $s(t)$, $c_n(t)$, $r(t)$, and N denote the original non-stationary signal, the separated IMFs, the residual, and the number of IMFs, respectively, the mathematical principle of EMD can be expressed as:

$$s(t) = \sum_{n=1}^N c_n(t) + r(t). \quad (6)$$

For a non-stationary signal $s(t)$, using equation 6, we get a finite set of subsignals $c_n(t), (n = 1, 2, \dots, N)$.

A special property of EMD is that the IMFs represent different oscillations embedded in the data, where the oscillating frequency for each subsignal $c_n(t)$ decreases as the sequence number of the IMF becomes larger (we call it a frequency decreasing property in the following context). This property results from the sifting algorithm used to implement the decomposition. Appendix A gives a detailed instruction about the sifting process, which can be summarized as a process in which low-frequency components are gradually removed to generate a more local-constant-frequency mode, which is followed by the generation of the next mode.

Figure 2 gives a demonstration for a synthetic signal. The original synthetic signal is generated through $d(t) = \sin(0.2\pi t) + \sin(0.4\pi t) + \sin(0.8\pi t)$; in other words, it is constructed from three individual frequency components corresponding to 0.1 Hz, 0.2 Hz and 0.4 Hz, respectively. From Figure 2, we can see that, except for small edge imprecision and negligible residual, EMD successfully decompose this signal into three components with a frequency ratio of approximately 4:2:1.

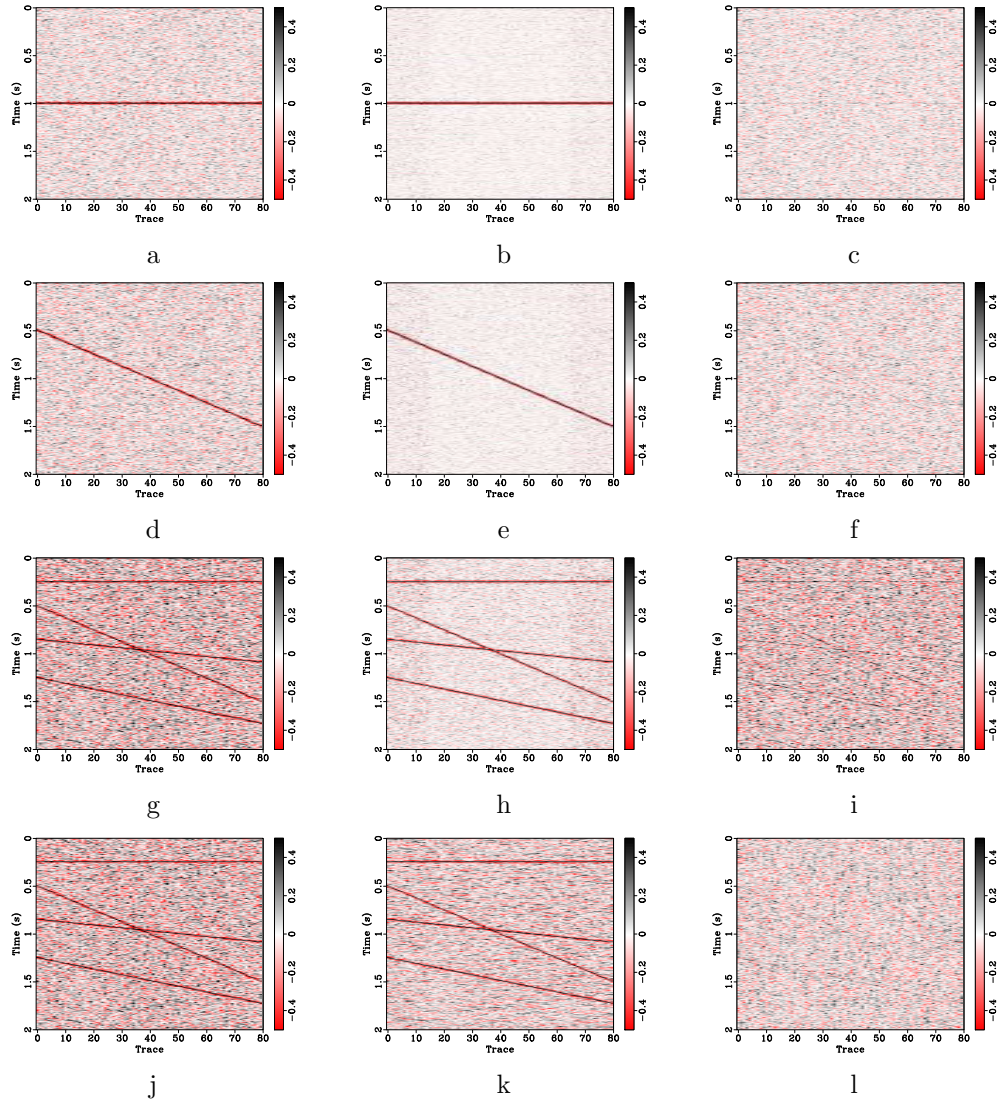


Figure 1: Demonstration of $f - x$ predictive filtering (a-i) and $f - x$ EMDPF (j-l) on synthetic section with different number of dip components. (a) Single flat event. (b) Noisy single flat event. (c) Removed noise section corresponding to (a) and (b). (d) Single dipping event. (e) Noisy single dipping event. (f) Removed noise section corresponding to (d) and (e). (g) Complex events section. (h) Noisy complex events section. (i) Removed noise section corresponding to (g) and (h). (j) Same as (g). (k) Denoised result by $f - x$ EMDPF. (l) Removed noise section corresponding to (j) and (k).

Because of the frequency decreasing property, EMD has been used outside geophysics for noise attenuation (Mao and Que, 2007; Kopsinis, 2009). Since random noise represents mainly the high-frequency components, by removing the IMFs with the highest frequency, we can attenuate this type of noise. However, in exploration geophysics, applying EMD to time traces is not effective because of the mode mixing problem. Kopecky (2010) defined mode mixing as any IMF consisting of frequencies of dramatically disparate scales. When mode mixing exists, the first one or two IMFs contain a lot of useful reflection energy. Extensions to EMD, such as ensemble empirical mode decomposition (EEMD) (Wu and Huang, 2009) and complete ensemble empirical mode decomposition (CEEMD) (Torres et al., 2011) have been proposed to solve the mode-mixing problem in signal processing and have been used in geophysics to analyze time-frequency properties, but have not been used for t - x domain seismic noise attenuation.

***f*-*x* EMD**

Instead of $t - x$ domain EMD, a $f - x$ domain EMD method to attenuate random noise in seismic data has been proposed by Bekara and van der Baan (2009). They apply EMD on each frequency slice in the $f - x$ domain, and suppress the higher wavenumber components, which mainly represent random noise. However, a problem occurs when applying $f - x$ EMD, because the high-wavenumber dipping events will also be removed. This problem occurs because, for many data sets, the random noise and any steeply dipping coherent energy make a significantly larger contribution to the high-wavenumber energy in the f - x domain than any desired signal (Bekara and van der Baan, 2009).

Bekara and van der Baan (2009) cleverly utilize this by-product of $f - x$ EMD to attenuate coherent noise such as ground roll.

The detailed algorithmic steps of $f - x$ EMD are given by Bekara and van der Baan (2009) as:

1. Select a time window and transform the data to the $f - x$ domain.
2. For every frequency,
 - (a) separate real and imaginary parts in the spatial sequence,
 - (b) compute IMF1, for the real signal and subtract it to obtain the filtered real signal,
 - (c) repeat for the imaginary part,
 - (d) combine to create the filtered complex signal.
3. Transform data back to the $t - x$ domain.
4. Repeat for the next time window.

$f - x$ EMD can be used as an adaptive $f - k$ filter. The cutoff wavenumber is adaptively defined and does not need any a priori knowledge about the seismic data in order to define the filter parameters. This adaptability makes $f - x$ EMD very convenient to utilize in real applications. The frequency-slice-dependent adaptability also makes $f - x$ EMD more precise than $f - x$ predictive filtering, because all the filter parameters in $f - x$ predictive filtering for each frequency slice are the same. Another advantage of $f - x$ EMD over $f - x$ predictive filtering is that the trace spacing does not need to be perfectly regular because no convolutional operator is used, a characteristic similar to local median and SVD filtering (Bekara and van der Baan, 2007, 2009).

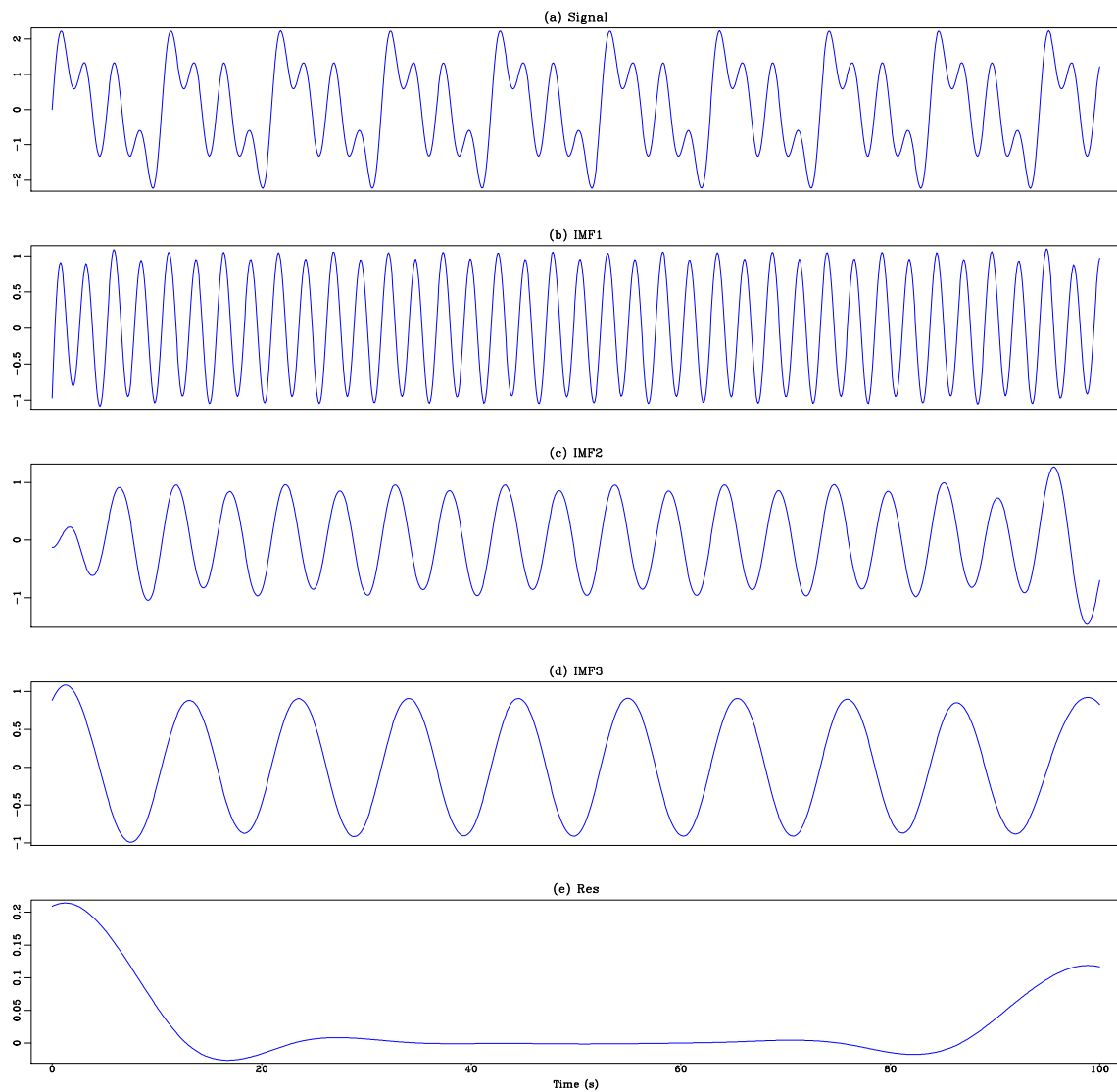


Figure 2: Demonstration of empirical mode decomposition on a synthetic signal. (a) The original signal, (b) first IMF, (c) second IMF, (d) third IMF, (e) residual.

***F-X* EMPIRICAL MODE DECOMPOSITION PREDICTIVE FILTERING**

$f-x$ EMDPF utilizes the property that the first few (generally 1 ~ 3) IMFs for each frequency slice in the $f-x$ domain contain the high-dip-angle components and random noise. Thus the leaked dipping events can be obtained by applying a predictive filter to these IMFs. Adding the predicted signal to the sum of the remaining IMFs will suppress random noise without harming the effective signals.

$F-x$ EMDPF is a new seismic noise attenuation method which combines the advantages of both $f-x$ predictive filtering and $f-x$ EMD. The detailed algorithmic steps of $f-x$ EMDPF are similar to $f-x$ EMD (Bekara and van der Baan, 2009) and are shown below:

1. Select a time window and transform the data to the $f-x$ domain.
2. For every frequency,
 - (a) separate real and imaginary parts in the spatial sequence,
 - (b) compute IMF1, for the real signal and subtract it to obtain the filtered real signal,
 - (c) apply an AR model to IMF1 and add the result to the sum of the remaining IMFs,
 - (d) repeat for the imaginary part,
 - (e) combine to create the filtered complex signal.
3. Transform data back to the $t-x$ domain.
4. Repeat for the next time window.

It should be emphasized that the number of the filtered IMFs is not limited to one, but is selected according to both the noise level and the distribution of the dip components within the specific seismic data set. If the noise level is high, then a larger number of IMFs should be chosen, because the noise remains not only in the first IMF but also in the second or the third, albeit with decreasing energy. If the dip components are mainly distributed in the high-angle range, then the number of IMFs could be relatively smaller, but when the dip components are distributed in the low- or mid-angle range, we should choose more IMFs in order to ensure that noise is removed whilst still preserving these dipping components.

Generally the number of IMFs for filtering is within the range of 1 ~ 3. In conventional EMD, the signal is completely decomposed into all the IMFs, along with the remainder. In our proposed algorithm, EMD decomposes a signal into only 1 ~ 3 components, which correspond to the number of IMFs to be filtered. Compared with the conventional EMD, this uncompleted decomposition algorithm can improve the computation efficiency by about 5 times.

EMD BASED DIP FILTER

In this section, we seek to connect $f - x$ EMDPF with $f - x$ predictive filtering and $f - x$ EMD. We would like to first introduce the so-called EMD based dip filter.

Since the frequency of each IMF decreases according to the order in which it is separated out, by subtracting the first few IMFs of each frequency slice in the $f - x$ domain, we extract the higher wavenumber components, which represent the energy of random noise and high-dip-angle events in seismic sections.

If we divide the set of IMFs into more-detailed zones, we can separate the section into several dip bands. Thus, we reach the definition of the EMD based dip filter:

$$\tilde{u}_i(f, h) = \begin{cases} \epsilon_1 u_i(f, h) & i \in D_1 \\ \epsilon_2 u_i(f, h) & i \in D_2 \\ \vdots & \vdots \\ \epsilon_m u_i(f, h) & i \in D_m \end{cases}, \quad (7)$$

$$\Lambda(f, h) = \sum_{i=1}^N \tilde{u}_i(f, h), \quad (8)$$

where $\Lambda(f, h)$ is the filtered data for frequency slice f in the $f - x$ domain. $u_i(f, h) (i = 1, 2, \dots, N)$ is the i th separated IMF such that $S(f, h) = \sum_{i=1}^N u_i(f, h)$, where $S(f, h)$ is the transformed $f - x$ domain seismic data. $D_i (i = 1, 2, \dots, m)$ is the i th of m , the number of dip bands, and ϵ_i is the corresponding weighting coefficient. For a simple high-pass dip filter, we choose $m = 2$, $\epsilon_1 = 1$, $\epsilon_2 = 0$ and $D_1 = \{1, 2\}$, $D_2 = \{3, 4, \dots, N\}$.

Figure 3 demonstrates how an EMD based dip filter works on a synthetic plane-wave seismic profile containing three events corresponding to three dips. After filtering with high-pass, mid-pass, and low-pass dip filters, respectively, the three plane waves are successfully separated. The parameters we choose in designing these three filters are shown in Table 1.

Type	N	m	ϵ	D
high-pass	10	2	$\epsilon_1 = 1, \epsilon_2 = 0$	$D_1 = \{1\}, D_2 = \{2, 3, \dots, 10\}$
mid-pass	10	3	$\epsilon_1 = 0, \epsilon_2 = 1, \epsilon_3 = 0$	$D_1 = \{1\}, D_2 = \{2\}, D_3 = \{3, 4, \dots, 10\}$
low-pass	10	2	$\epsilon_1 = 0, \epsilon_2 = 1$	$D_1 = \{1\}, D_2 = \{2, 3, \dots, 10\}$

Table 1: Parameters in designing high-pass, mid-pass and low-pass dip filters corresponding to Figure 3.

The EMD based dip filter is defined adaptively since the filtering process is data driven. We only need to define the number of IMFs contained in each dip band at the start, a step that is convenient to implement.

If we consider random noise as high-dip-angle components, then $f - x$ EMD denoising (Bekara and van der Baan, 2009) is equivalent to applying a high-cut dip filter with the form of equation 7 to the seismic data in order to remove both random noise and ground roll. We can also understand $f - x$ EMDPF from EMD based dip filter. $f - x$ EMDPF first uses an EMD based dip filter to separate the high-dip-angle and low-dip-angle components, where the high-dip-angle components are composed of steeply dipping useful events and noise, and low-dip-angle components are all useful signals. The useful signal in the high-dip-angle components are predicted and subsequently restored. Due to the effects of the EMD based dip filter, a decrease occurs in the number of useful signal components that needs to be predicted. This decrease results in more accurate overall performance when compared with conventional predictive filtering.

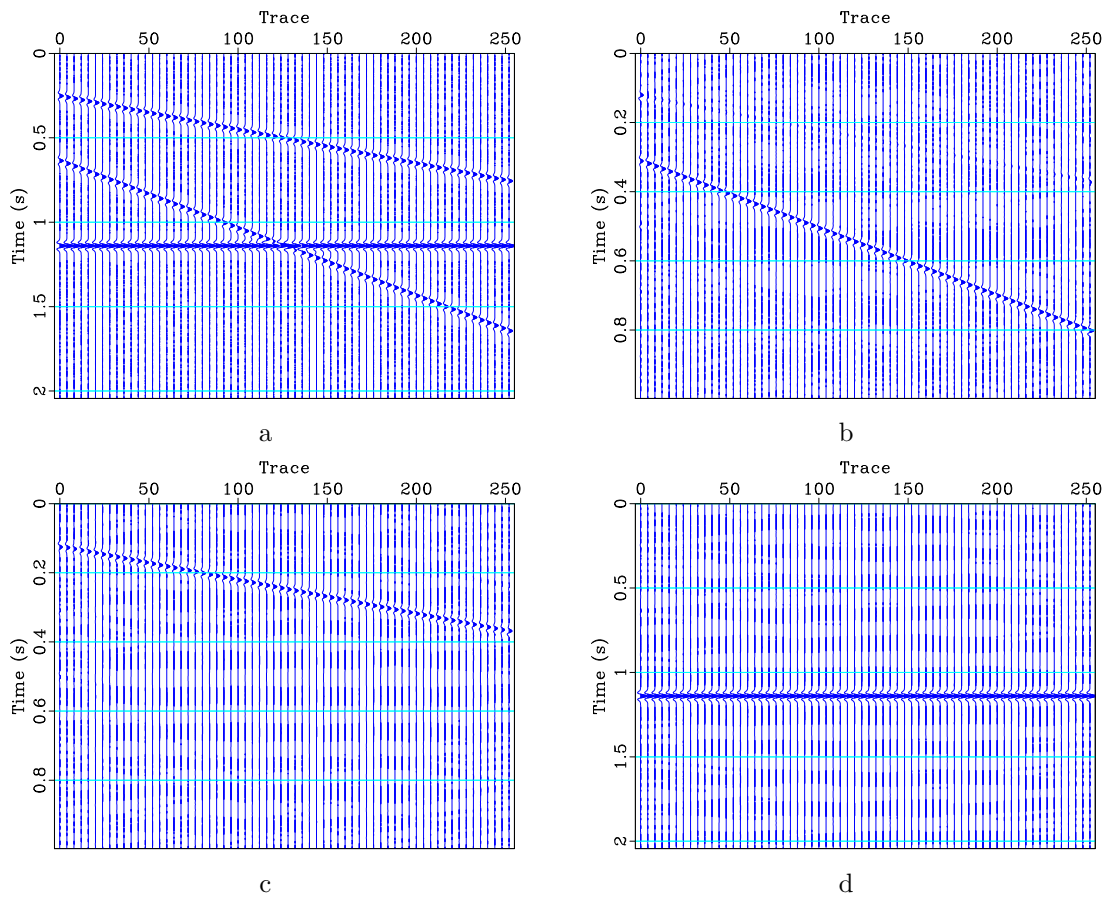


Figure 3: Demonstration of EMD based dip filter. (a) Original synthetic profile, (b) with high-pass dip filter, (c) with mid-pass dip filter, (d) with low-pass dip filter.

EXAMPLES

In this section, we first reuse the previously discussed synthetic data (Figure 1j), then show two other synthetic data and one field data example to demonstrate the

performance of $f - x$ EMDPF.

Figure 1k shows the denoised result after $f - x$ EMDPF. The removed noise section is shown in Figure 1l. Comparing Figure 1i and Figure 1l, we see that the useful events leaked into Figure 1i have been returned to the denoised result (Figure 1k), while the noise level stays nearly unchanged.

The second synthetic example is composed of one linear dipping event and two flat events (Figure 4). A 40 Hz Ricker wavelet has been used with a time sample interval of 4 ms. The number of samples for each trace is 501, and the number of traces is 120. Figures 4d, 4e, and 4f illustrate the comparison of denoised results of the synthetic data using $f - x$ predictive filtering, $f - x$ EMD filtering, and $f - x$ EMDPF, respectively. Figure 4a is the noise free data, Figure 4b is Gaussian white noise, and Figure 4c is the noisy data. The SNR of the noisy data is 2.0 (using the previous definition of SNR). Figures 4g, 4h, and 4i show the removed noise sections corresponding to $f - x$ predictive filtering, $f - x$ EMD, and $f - x$ EMDPF, respectively. From Figure 4g, we can see that $f - x$ predictive filtering harms both flat and dipping events to some extent. Although by increasing the length of the predictive step we can decrease the damage done to the signals, the noise suppression is less effective because of the stronger prediction of noise. Also, as seen in Figure 4d, the $f - x$ predictive filtering introduces some artefacts. In Figure 4h, we see that $f - x$ EMD tends to harm much of the dip energy but preserves entirely the flat events. Using the same predictive filtering parameters, we see from Figure 4i that both flat and dipping signals are hardly affected when $f - x$ EMDPF is applied. In this example, the first IMF is removed for prediction in the process of $f - x$ EMDPF. Figure 5 demonstrates the sensitivity of the $f - x$ EMDPF for increasing the number of filtered IMFs. We can see that, as the number of filtered IMFs increases, the denoising result becomes more similar to $f - x$ predictive filtering; that is, more noise is removed and more obvious artefacts appear in the denoised section. However, for $f - x$ EMDPF, the horizontal events are always totally preserved, which supposes a generally better denoising result than $f - x$ predictive filtering.

The third synthetic example is a benchmark data set from SeismicLab. The central frequency of the Ricker wavelet is 40 Hz and the temporal sampling is 2 ms. The number of time samples is 750 and the number of spatial samples is 50. Figures 6a, 6b, and 6c denote the clean data, noise section, and noisy section, respectively. The SNR in Figure 6c is 2.0. Figures 6d, 6e, and 6f are the denoised results using $f - x$ predictive filtering, $f - x$ EMD, and $f - x$ EMDPF, respectively. From removed noise sections Figures 6g, 6h, and 6i we can conclude that $f - x$ predictive filtering harms much useful energy when the number of dip components increases, whereas $f - x$ EMD affects most of the dipping events, and $f - x$ EMDPF preserves the useful energy to the greatest extent while removing the slightly weaker level of noise. In this example, the first IMF is removed for prediction in the process of $f - x$ EMDPF.

The field data is shown in Figure 7. It is a stacked section without migration from the South China Sea. Figure 7b is a zoomed portion of Figure 7a from 1.5s to 3.0s. The denoised profiles, shown in Figures 8a, 8c, and 8e, demonstrate $f - x$

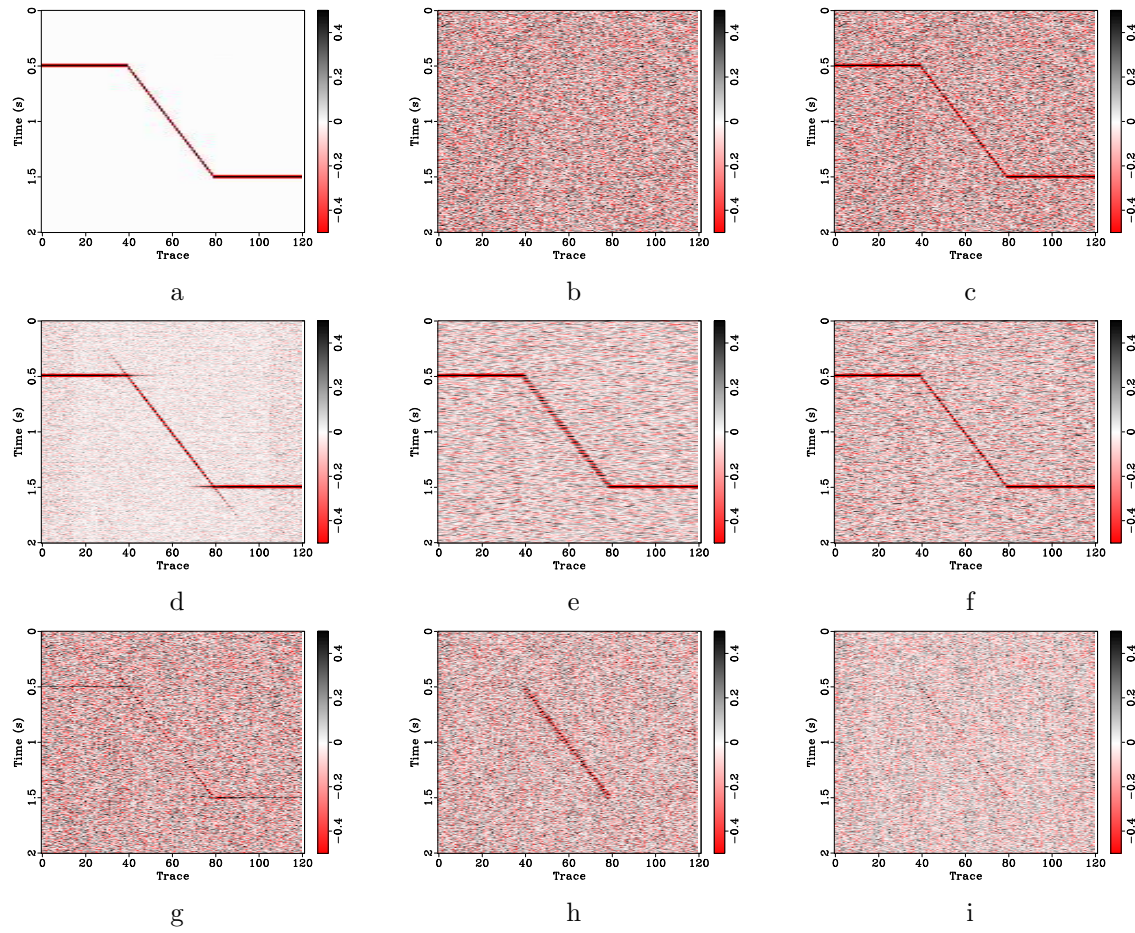


Figure 4: Comparison of denoising effects. (a) Clean data. (b) Gaussian white noise. (c) Noisy data. (d) Denoised result by $f - x$ predictive filtering. (e) Denoised result by $f - x$ EMD. (f) Denoised result by $f - x$ EMDPF. (g) Removed noise section corresponding to (d). (h) Removed noise section corresponding to (e). (i) Removed noise section corresponding to (f).

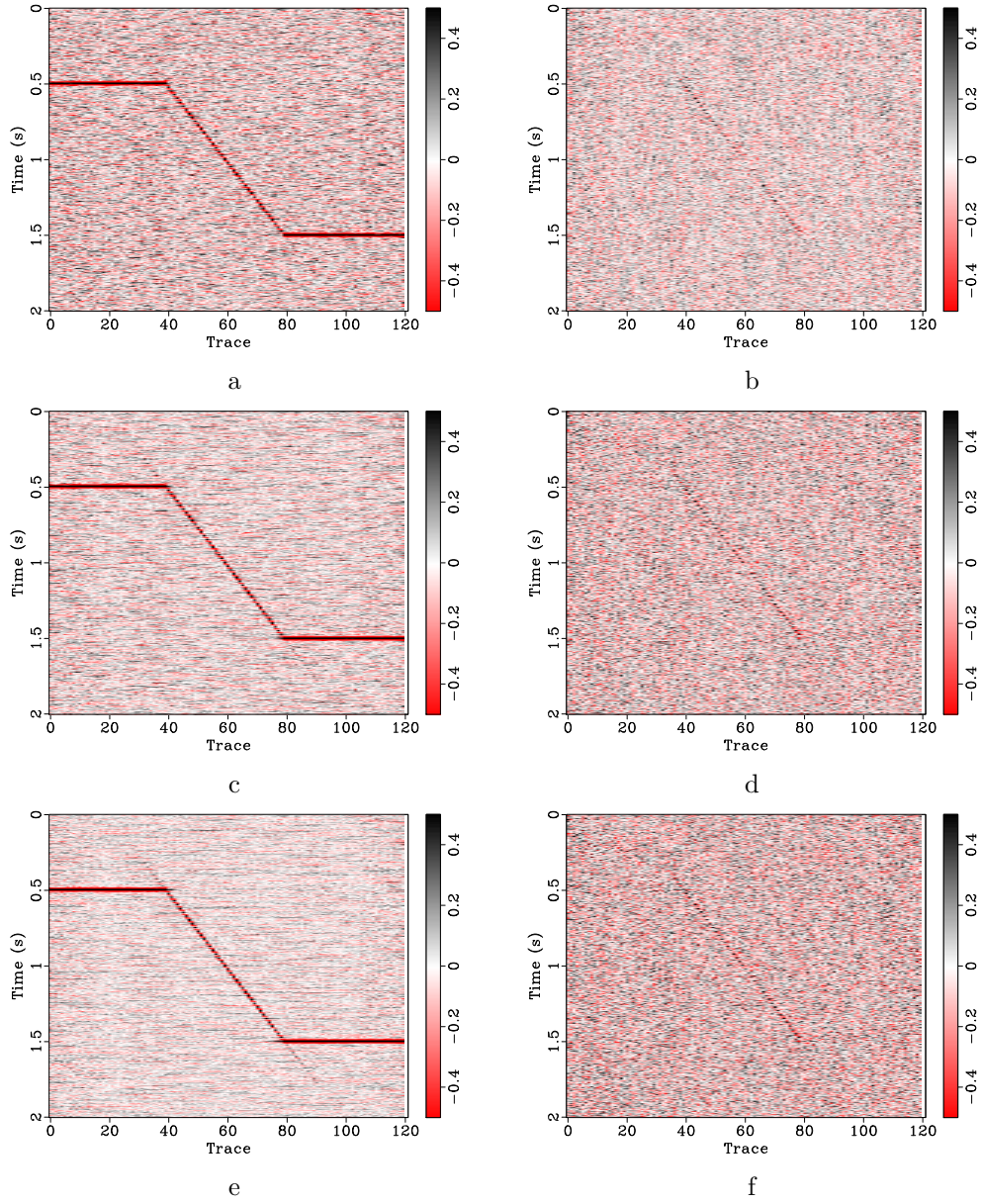


Figure 5: Comparison of denoising effects. (a) $f - x$ EMDPF denoised result with prediction on 1 IMF. (b) Noise section corresponding to (a). (c) $f - x$ EMDPF denoised result with prediction on 2 IMFs. (d) Noise section corresponding to (c). (e) $f - x$ EMDPF denoised result with prediction on 3 IMFs. (f) Noise section corresponding to (e).

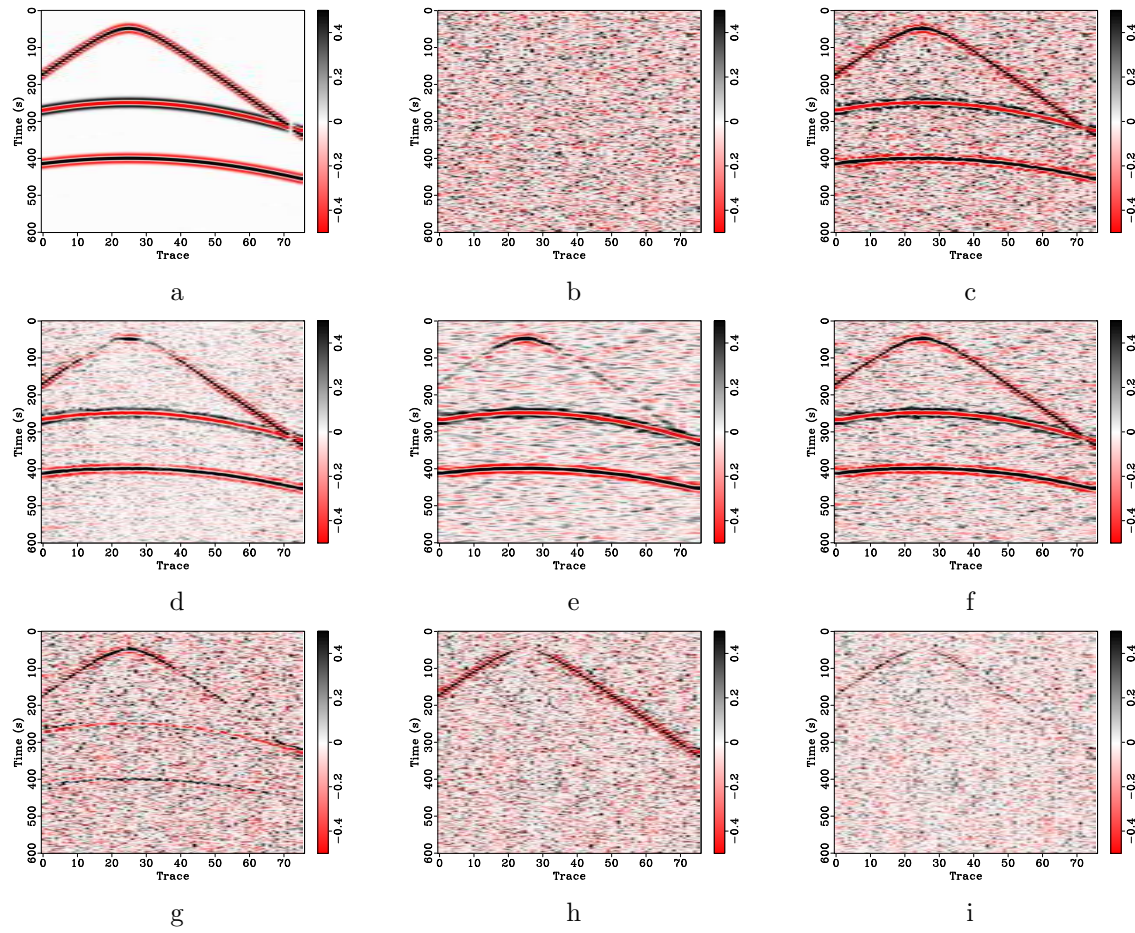


Figure 6: Comparison of denoising effects. (a) Clean data. (b) Gaussian white noise. (c) Noisy data. (d) Denoised result by $f - x$ predictive filtering. (e) Denoised result by $f - x$ EMD. (f) Denoised result by $f - x$ EMDPF. (g) Removed noise section corresponding to (d). (h) Removed noise section corresponding to (e). (i) Removed noise section corresponding to (f).

predictive filtering, $f - x$ EMD, and $f - x$ EMDPF, respectively. The corresponding noise sections are shown in Figures 8b, 8d, and 8f. From these noise sections, we see clearly that $f - x$ EMD removes many dipping events. Even though we can't see clearly the improvement after applying $f - x$ EMDPF at the scale of Figure 8, the improvement can be identified on the zoomed noise sections shown in Figure 9. The useful energy shown around 1.75s, 2.6s in Figure 9b does not exist in the same part of Figure 9f. From these differences, we conclude that $f - x$ EMDPF is more satisfactory than $f - x$ predictive filtering and $f - x$ EMD, in that it leaves less useful energy in the noise section. In this real data example, we apply the AR model on the first three IMFs for $f - x$ EMDPF. For display reasons, the noise sections have been amplified by 3 times.

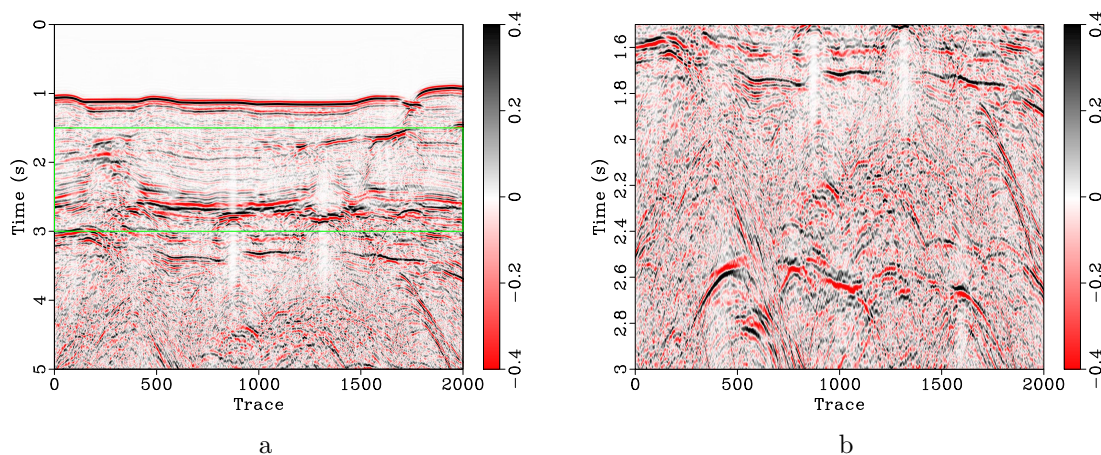


Figure 7: Field data from the South China Sea. (a) Original post-stack pre-migration profile. (b) Temporal zoomed part from 1.5s to 3.0s.

CONCLUSIONS

We have proposed a new denoising method suitable for complex subsurface structures. We demonstrate that the number of dipping events will affect the denoising performance of $f - x$ predictive filtering. We also give the definition of an EMD based dip filter and ascribe the effectiveness of $f - x$ EMD to applying a high-cut EMD based dip filter to seismic profiles.

By using the AR model to predict the steeply dipping event, $f - x$ EMDPF can deal with complex seismic profiles that conventional $f - x$ EMD can't handle. By applying an EMD based adaptive dip filter in advance, $f - x$ EMDPF can preserve more useful energy as compared with conventional $f - x$ predictive filtering. $f - x$ EMDPF is actually a modification to both $f - x$ predictive filtering and $f - x$ EMD, so it maintains the benefits of being convenient, data driven, whilst combining the dip-selection property of EMD with the power of the AR model used in $f - x$ predictive filtering.

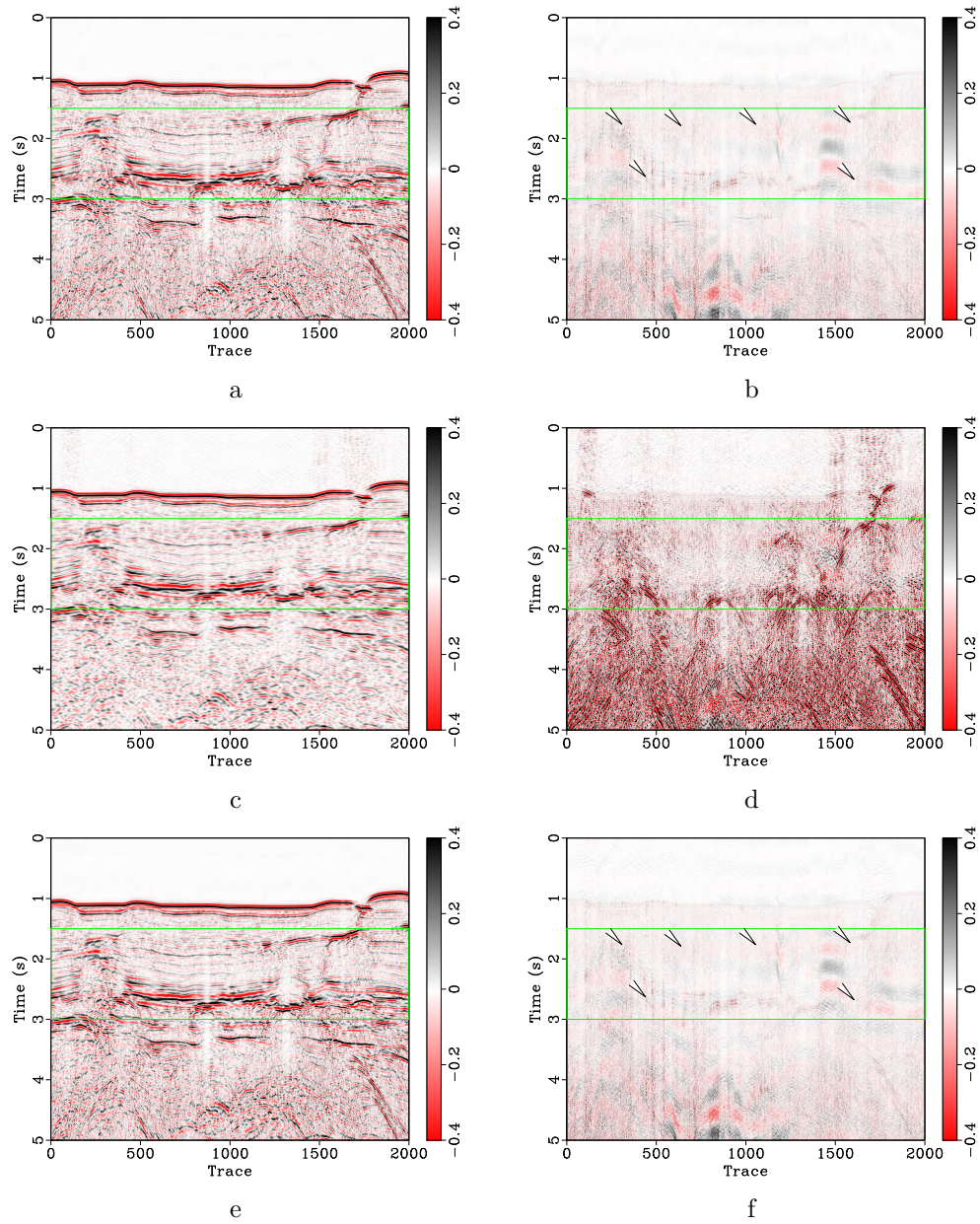


Figure 8: Comparisons between denoised results and corresponding noise sections. (a) Denoised result by $f - x$ predictive filtering. (b) Removed noise section by $f - x$ predictive filtering ($\times 3$). (c) Denoised result by $f - x$ EMD. (d) Removed noise section by $f - x$ EMD ($\times 3$). (e) Denoised result by $f - x$ EMDPF. (d) Removed noise section by $f - x$ EMDPF ($\times 3$).

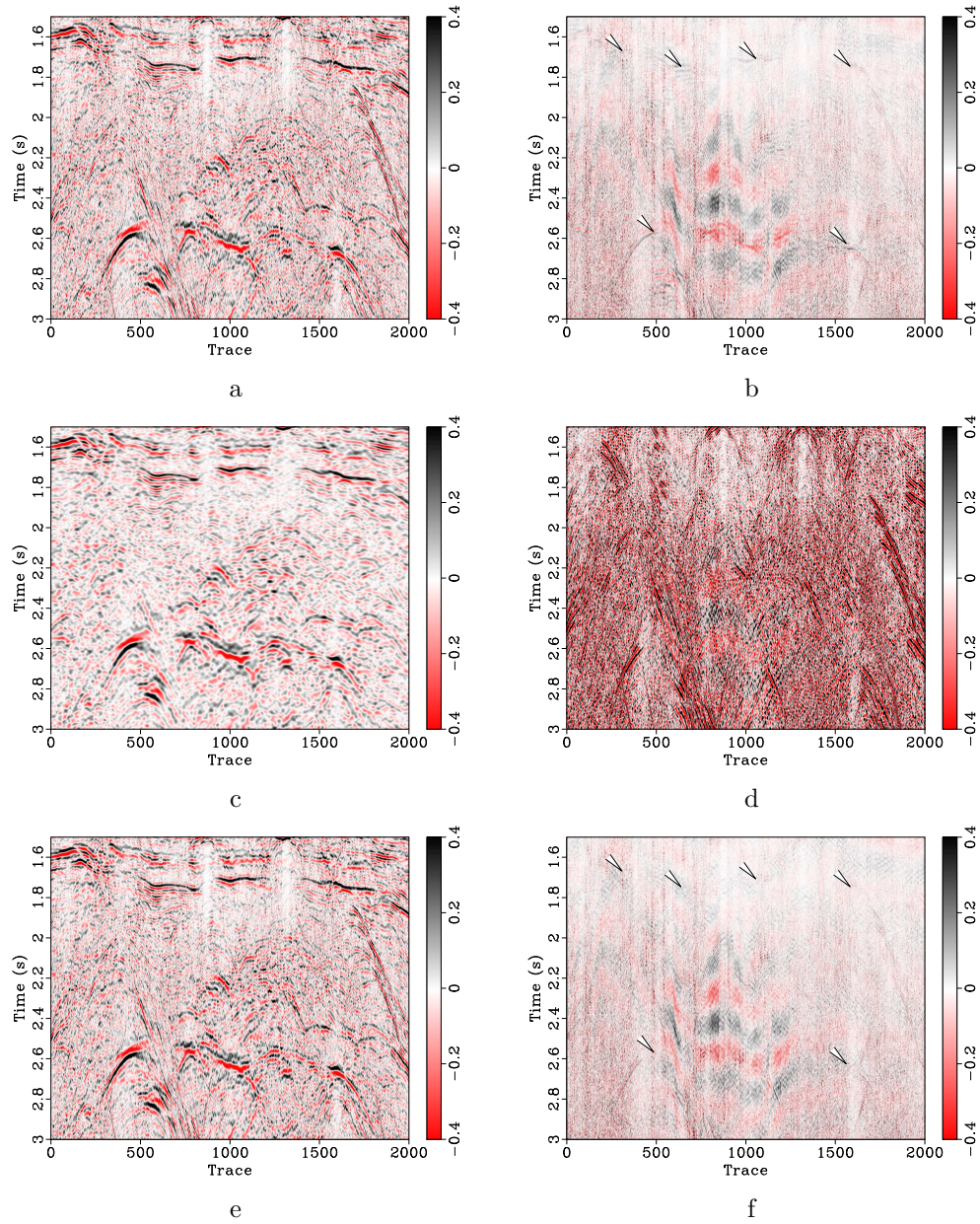


Figure 9: Zoomed part of denoised results and corresponding noise sections. (a) Denoised result by $f - x$ predictive filtering. (b) Removed noise section by $f - x$ predictive filtering ($\times 3$). (c) Denoised result by $f - x$ EMD. (d) Removed noise section by $f - x$ EMD ($\times 3$). (e) Denoised result by $f - x$ EMDPF. (f) Removed noise section by $f - x$ EMDPF ($\times 3$).

Although the incomplete EMD described in this paper can improve computational efficiency, a great deal of time is still required to process the data. Currently, this time requirement is the major drawback of the approach. In addition, continued research is required in order to find an efficient thresholding method in the $f - x$ domain in order to improve the preservation of useful signal.

ACKNOWLEDGEMENTS

We thank Josef Paffenholz, Mauricio Sacchi, Sergey Fomel, and Karl Schleicher for helpful discussions and all the developers of Madagascar and SeismicLab software packages for providing the codes. We also thank the associate editor Danilo Velis and three anonymous reviewers for their constructive suggestions, which helped to improve the paper.

REFERENCES

- Bekara, M., and M. van der Baan, 2007, Local singular value decomposition for signal enhancement of seismic data: *Geophysics*, **72**, V59–V65.
- , 2009, Random and coherent noise attenuation by empirical mode decomposition: *Geophysics*, **74**, V89–V98.
- Cai, H., Z. He, and D. Huang, 2011, Seismic data denoising based on mixed time-frequency methods: *Applied Geophysics*, **8**, 319–327.
- Canales, L., 1984, Random noise reduction: SEG expanded abstracts:54th Annual international meeting, 525–527.
- Fomel, S., and Y. Liu, 2010, Seislet transform and seislet frame: *Geophysics*, **75**, V25–V38.
- Gao, J., J. Mao, W. Chen, and Q. Zheng, 2006, On the denoising method of prestack seismic data in wavelet domain: *Chinese J. Geophys*, **49**, 1155–1163.
- Guo, J., X. Zhou, and H. Yang, 1995, Attenuation of random noise in $f-x, y$ domain: *Oil Geophysical Prospecting*, **30**, 207–215.
- Harris, P., and R. White, 1997, Improving the performance of f-x prediction at low signal-to-noise ratios: *Geophysical Prospecting*, **45**, 269–302.
- Huang, N. E., Z. Shen, S. R. Long, M. C. Wu, H. H. Shih, Q. Zheng, N.-C. Yen, C. C. Tung, and H. H. Liu, 1998, The empirical mode decomposition and the Hilbert spectrum for nonlinear and non-stationary time series analysis: *Proceeding of the Royal Society of London Series A*, **454**, 903–995.
- Kang, Y., C. Yu, W. Jia, and C. Wang, 2003, A study on noise-suppression method in f-x domain: *Oil Geophysical Prospecting*, **38**, 136–138.
- Kopecky, M., 2010, Ensemble empirical mode decomposition: Image data analysis with white-noise reflection: *Acta Polytechnica*, **50**, 49–56.
- Kopsinis, Y., 2009, Development of EMD-based denoising methods inspired by wavelet thresholding: *Signal Processing, IEEE Transactions on*, **57**, 1351 – 1362.
- Liu, C., H. Li, C. Tao, Y. Liu, D. Wang, and C. Gu, 2007, A new fuzzy nesting

- multilevel median filter and its application to seismic data processing: Chinese J. Geophysics, **50**, 1534–1542.
- Liu, G., X. Chen, J. Du, and J. Song, 2011, Seismic noise attenuation using nonstationary polynomial fitting: Applied Geophysics, **8**, 18–26.
- Liu, G., S. Fomel, L. Jin, and X. Chen, 2009a, Stacking seismic data using local correlation: Geophysics, **74**, V43–V48.
- Liu, Y., S. Fomel, C. Liu, D. Wang, G. Liu, and X. Feng, 2009b, High-order seislet transform and its application of random noise attenuation: Chinese J. Geophysics, **52**, 2142–2151.
- Liu, Z., X. Chen, and J. Li, 2009c, Noncasual spatial prediction filtering based on an ARMA model: Applied Geophysics, **6**, 122–128.
- Mao, Y., and P. Que, 2007, Noise suppression and flawdetection of ultrasonic signals via empirical mode decomposition: Rus. J. Nondestruct. Test., **43**, 196–203.
- Mayne, W., 1962, Common reflection point horizontal data stacking techniques: Geophysics, **27**, 927–938.
- Neelamani, R., A. Baumstein, D. Gillard, M. Hadidi, and W. Soroka, 2008, Coherent and random noise attenuation using the curvelet transform: The Leading Edge, **27**, 240–248.
- Sacchi, M. D., 2008, <http://seismic-lab.physics.ualberta.ca/>: SeismicLab.
- Su, G., X. Zhou, and C. Li, 1998, Prediction noise elimination in f - xyz domain: Oil Geophysical Prospecting, **33**, 95–103.
- Torres, M. E., M. A. Colominas, G. Schlotthauer, and P. Flandrin, 2011, A complete ensemble empirical mode decomposition with adaptive noise: IEEE International Conference on Acoustics, Speech and Signal Processing (ICASSP), 4144–4147.
- Tufts, D., and R. Kumaresan, 1980, Estimation of frequencies of multiple sinusoids: Making linear prediction perform like maximum likelihood: Proceedings of the IEEE, **70**, 975–989.
- Wu, Z., and N. E. Huang, 2009, Ensemble empirical mode decomposition: A noise-assisted data analysis method: Advances in Adaptive Data Analysis, **01**, 1–41.
- Yilmaz, O., 2001, Seismic data analysis: Processing, inversion, and interpretation of seismic data: Soc. Expl. Geophys.
- Zhang, R., and T. Ulrych, 2003, Physical wavelet frame denoising: Geophysics, **68**, 225–231.
- Zhong, W., B. Yang, and Z. Zhang, 2006, Research on application of polynomial fitting technique in highly noisy seismic data: Progress in Geophysics, **21**, 184–189.

APPENDIX A: SIFTING ALGORITHM FOR EMPIRICAL MODE DECOMPOSITION

In this appendix, we review the sifting algorithm of empirical mode decomposition (equation 6 in the main paper). For the original signal, we first find the local maxima and minima of the signal. Once identified, fit these local maxima and minima by

cubic spline interpolation in turn in order to generate the upper and lower envelopes. Then compute the mean of the upper and lower envelopes m_{11} , the difference between the data and first mean h_{11} .

$$m_{11} = \frac{h_{10}^+ + h_{10}^-}{2}, \quad (\text{A-1})$$

$$h_{11} = h_{10} - m_{11}, \quad (\text{A-2})$$

where h_{ij} denotes the remaining signal after j th sifting for generating the i th IMF, h_{ij}^+ and h_{ij}^- are corresponding upper and lower envelopes, respectively, and m_{ij} is the mean of upper and lower envelopes after j th sifting for generating the i th IMF. Repeating the sifting procedure (A-2) k times, until h_{1k} reach the prerequisites of IMF, these are:

$$h_{1(k-1)} - m_{1k} = h_{1k}. \quad (\text{A-3})$$

The criterion for the sifting process to stop is given by Huang et al. (1998) as:

$$0.2 \leq SD = \sum_{t=0}^T \left[\frac{|h_{1(k-1)}(t) - h_{1k}(t)|^2}{h_{1(k-1)}^2} \right] \leq 0.3, \quad (\text{A-4})$$

where SD denotes the standard deviation. When h_{1k} is considered as an IMF, let $c_1 = h_{1k}$, we separate the first IMF from the original data:

$$d - c_1 = r_1, \quad (\text{A-5})$$

where d is the original signal, c_n denotes the n th IMF, and r_n is the residual after the n th IMF based sifting. Repeating the sifting process from equation A-1 to A-5, changing h_{1j} to h_{ij} , in order to get the following IMFs: c_2, c_3, \dots, c_N . The sifting process can be stopped when the residual r_n , becomes so small that it is less than a predetermined value of substantial consequence, or when r_n becomes a monotonic function from which no more IMF can be extracted.

Finally, we achieved a decomposition of the original data into N modes, and one residual, as shown in equation 6 in the main context.